Semiconductor Optoelectronics
ISSN: 1001-5868

TUNING THE OPTICAL BAND GAP OF HALF-DOPED $LA_{0.5}$ $SR_{0.5}MNO_3$ NANOCRYSTALLITES BY ANNEALING AT DIFFERENT TEMPERATURES.

Mohd Abdul Shukur[1,2], K. Vijaya Kumar[1*], G. Narsinga Rao[3]
[1]Department of Physics, JNTUH University College of Engineering Rajanna Sircilla, Agraharam, Rajanna Sircilla – District, 505301, Telangana, India.
[2]Department of Physics, SRR Government Arts & Science College (Autonomous), Karimnagar, 505001, Telangana, India
[3]Department of Physics, Marri Laxman Reddy Institute of Technology and Management, Dundigal, Hyderabad 500043, Telangana, India.

Abstract
The perovskite nanocrystallites of Strontium doped lanthanum manganite $La_{0.5}Sr_{0.5}MnO_3$ were synthesized using the combustion method and subsequently subjected to annealing at temperatures of 600, 800, 1000, and 1200°C for a duration of 6 hours. These are characterized by X-ray diffractometry (XRD) and UV-Vis spectrometry. The XRD displays growth of a Rhombohedral, space group $3\bar{R}C$ structure in the nanocrystallites, with no impurity peaks observed except in the sample annealed at 600°C. The average size of the crystallites was found to increase gradually from 15 to 30nm as a function of annealing temperature. Analysis of the UV-Vis spectra revealed that the optical gap of the $La_{0.5}Sr_{0.5}MnO_3$ nanocrystallite materials were decreased from 3.02 to 2.48eV with the rise in annealing temperature. This implies that the $La_{0.5}Sr_{0.5}MnO_3$ nanocrystallites exhibit semiconductor properties. Therefore, the annealing of $La_{0.5}Sr_{0.5}MnO_3$ nanocrystallites at different temperatures resulted in the emergence of unique optical characteristics.

Keywords: Crystallite Size, Tauc plot, Reflectance, Moss relation, Herve and Vandamme relation

Corresponding Author: kvkphd@gmail.com (K. Vijaya Kumar)

Introduction

Perovskite structured Manganite denoted as $Re_{1-x}A_xMnO_3$ where Re represents Rare-earth metal ions such as La, Nd, Pr etc and A represents Alkaline earth ion such as Sr, Ca, Ba, etc, exhibit a distinct kind of structural, and optical properties. “The interactions between charge, orbital, and lattice degrees of freedom give rise to different phases [1] and intricate phenomena such as superconductivity, colossal magnetoresistance (CMR), catalytic properties, magnetocaloric effect (M) led to “numerous technological applications in storage devices, bolometers, and solid oxide fuel cells (SOFC)”, while also attracting significant interest in the field of physics [7–9].These manganite exhibit diverse transport and magnetic properties, including “charge ordering (CO), orbital ordering (OO), Jahn-Teller (JT) effects, double exchange (DE) interactions, super exchange (SE) interactions, and the coexistence of different

phases" [10]. Doping at the Rare-earth metal ions sites or Alkaline-earth ion site enables the manipulation of Mn-O bond length and Mn-O-Mn bond angles. [11,12]. This substitution influences factors like tolerance factor, size mismatch, and oxygen stoichiometry, leading to distortions in the MnO_6 octahedra [13].

Extensive research has been conducted on lanthanum manganite doped with strontium ($La_{1-x}Sr_xMnO_3$) due to their potential usage as "cathodes in solid oxide fuel cells (SOFC), room temperature magnetic sensors, recording devices, and as bottom electrodes in the production of ferroelectric memories" [14, 15]. In its undoped form, lanthanum manganite ($LaMnO_3$) is a ferromagnetic insulator. However, by doping strontium at the lanthanum site, Mn^{3+} ions are converted to Mn^{4+} ions in a proportion equivalent to the doping level. This conversion enhances the double exchange (DE) interaction within the crystal structure. $La_{1-x}Sr_xMnO_3$ possesses a pseudo cubic structure and exhibits paramagnetic insulator (PMI) behaviour at greater temperatures, while transitioning to a ferromagnetic metal (FMM) state at lower temperatures [16].

The $La_{1-x}Sr_xMnO_3$ system displays different fundamental states depending on the level of Sr doping. In the range of $0.15 < x < 0.5$, the ground state is characterized as a ferromagnetic (FM) metal. However, with increasing x value above 0.5, behaves an antiferromagnetic (AFM) state [17]. In the half-doped $La_{0.5}Sr_{0.5}MnO_3$ crystallites, a transition from a metal to an insulator was observed, but no distinct conversion between the ferromagnetic (FM) and antiferromagnetic (AFM) states was detected [17].In polycrystalline $La_{0.5}Sr_{0.5}MnO_3$, charge ordering and a shift from ferromagnetic (FM) to antiferromagnetic (AFM) behavior were observed at lower temperatures, while a changeover from a metal to an insulator was not observed [18]. At a temperature of $T_N = 220$ K, an FM-AFM transition took place, accompanied by indications of charge ordering. However, no metal-insulator transition was observed [19]. Another study reported a clear transition from the ferromagnetic (FM) to the antiferromagnetic (AFM) state at a temperature of $T_N = 135$ K, with metallic behavior exhibited by the material and a noticeable change at 320 K [20]. The reported magnetic and electrical properties in these studies present distinct observations, which continue to be a subject of debate $La_{0.5}Sr_{0.5}MnO_3$, situated at the phase boundary as a half-doped sample, has been extensively explored in terms of its optical, electrical, and magnetic transport properties. The macroscopic physical properties of materials can be significantly affected by various external factors, such as annealing atmosphere, morphologies, and chemical substitution disorder. Among these factors, the annealing temperature plays a crucial role in controlling specific physical properties in manganite samples. The presence of the exchange bias effect in nanoparticles of half-doped manganite depended on the particle size, which, in turn, was influenced by different annealing temperatures [21]. Similarly, the size of the grains noticeably influenced the charge ordering and exchange bias in $Pr_{0.5}Ca_{0.5}MnO_3$ [22]. In the $La_{1-x}Sr_xMnO_3$ system, the optical properties are influenced by the quantum confinement effect, which arises due to the reduced dimensions of the particles. This effect leads to a shift in the energy bandgap of the material, causing the nanoparticles to exhibit different optical behavior compared to the bulk material. The impact of annealing temperatures on the optical properties of $La_{0.5}Sr_{0.5}MnO_3$ nanocrystallites has not been thoroughly explored in recent studies. Therefore, we conducted a systematic investigation to examine the impression of annealing temperature on the structural and optical properties, specifically the band gap and optical conductivity. For the preparation of the nanocrystallites,

we employed the combustion method due to its simplicity, high purity, and the ability to control chemical compositions effectively. This method allowed us to produce a large quantity of $La_{0.5}Sr_{0.5}MnO_3$ nanocrystals, even with small amounts of starting materials [23]. Our study involved subjecting the nanocrystallites to annealing temperatures of 600, 800, 1000, and 1200℃. We utilized various analytical devices to evaluate different parameters, aiming to gain a comprehensive understanding of how temperature influences the characteristics of $La_{0.5}Sr_{0.5}MnO_3$ nanocrystallites.

Experimental

Nanocrystallites $La_{0.5}Sr_{0.5}MnO_3$were synthesized by the combustion method from the precursors of nitrates such as Lanthanum nitrate [$La(NO_3)_36H_2O$], Strontium nitrate [$Sr(NO_3)_2$] and Manganese nitrates [$Mn(NO_3)_2.4H_2O$] (99% purity AR grade) as reactants using ethylene glycol ($C_2H_6O_2$), citric acid ($C_6H_8O_7$) as gelatinizer and chelating agent respectively. The chemical equation representing the stoichiometry of the preparation of $La_{0.5}Sr_{0.5}MnO_3$ from their nitrate precursors can be written as follows:

$$2La(NO_3)_3 + Sr(NO_3)_2 + 5Mn(NO_3)_2 + 10C_6H_8O_7 \rightarrow La_{0.5}Sr_{0.5}MnO_3 + 16CO_2 + 22H_2O$$

The required amounts of lanthanum nitrate, Manganese nitrate, Strontium nitrate in stoichiometric proportions were weighed and dissolved in a small volume of deionized water in a separate beaker. The stoichiometric volume of ethylene glycol and citric acid are added slowly to the nitrate solution with constant stirring. The citric acid, ethylene glycol, and metal nitrate were mixed in a molar ratio 4:3:1. A little quantity of ammonia was mixed into the combined solution to bring the pH level down to 7.0, producing a pink solution. This mixed solution was heated continuously about 80℃ with constant stirring on the magnetic stirrer until H_2O evaporation and formation of a glutinous gel. Citric acid and nitrates undergo a poly-condensation reaction through the dehydration process, resulting in the development of the gel. The gel is continuously heated at around 300℃ until the ignition started. As soon as the gels were lit, they began to burn in a self-propagating combustion process, which continued until all the gels had been consumed, leaving behind a loose, porous product [25]. This is the combustion process that produces a lot of heat and gas. Finally, the $La_{0.5}Sr_{0.5}MnO_3$ powder is obtained by annealing the dried ash at a temperature of 600,800,1000 and 1200℃ for 6 hours in a muffle furnace. This resulted in the production of $La_{0.5}Sr_{0.5}MnO_3$ nanocrystals with varying sizes. Finally, 1.5% PVA, which served as a binder, was completely mixed into the annealed powders before being crushed into pellets at a pressure of 5 tonnes per cm^2, with a 10mm diameter and a 2-3mm thickness. For a duration of four hours, the pellets underwent annealing at a temperature of 600,800,1000 and 1200℃ for 4 hours in a muffle furnace for 4 hours. The phase identification and crystallite size of the $La_{0.5}Sr_{0.5}MnO_3$ nanocrystals were determined using an X-ray powder diffractometer equipped with CuKα incident radiation with a wavelength of 1.54 A^ousing Rigaku X ray diffractometer, employing a step size of 0.02 degrees within the 2θ value from 20^{o}to 80^o. To assess the optical parameters, UV-Vis spectroscopy was performed using a SYSTRONICS DOUBLE BEAM spectrophotometer. The optical absorbances were obtained by ultrasonically dispersing a small quantity of the sample in distilled water. The data was then collected within the wavelength range of 200-800 nm.

XRD Analysis:

The pattern of XRD of $La_{0.5}Sr_{0.5}MnO_3$ nanocrystallites annealed at 600, 800, 1000 and 1200℃

were shown in the figure 1. The prominent peak for all samples were observed for the plane (104), (110) at Bragg's angle (2θ) around 32.7°, which reveals the $La_{0.5}Sr_{0.5}MnO_3$ nanocrystallites are perovskite structure [24], and which were in good agreement with the diffraction patterns indexed with the JCPDS # 00-051-0118. Theses observed diffraction peaks confirmed the formation of single-phase crystalline nature of rhombohedral structure $R\bar{3}C$ (167) space group without any impurities except for sample at 600°C. XRD of the sample at 600°C indicates a very minor peak at 25° and 36° related to an impurity phase as shown in the figure 1. It suggests that much of the aerosol gel had gone through the chemical reaction and the perovskite structure was formed at annealed temperature 600°C. But the contaminated impurity diffraction peak disappears with further annealing temperature above 600°C, which indicating a better absolute chemical reaction was attained at higher temperatures. The observed intensity of the prominent peak was maximum for sample at 1200°C due to high electron density. The average crystallite size $\langle D \rangle$ were measured by the Scherrer's formula [25].

$$\langle D \rangle = \frac{K\lambda}{\beta \cos\theta} \quad \ldots\ldots\ldots\ldots\ldots\ldots\ldots (1)$$

where, K is the shape factor (=0.9), λ=1.5418 Å (Wavelength of X ray radiation) and β =FWHM (Full width half maximum).

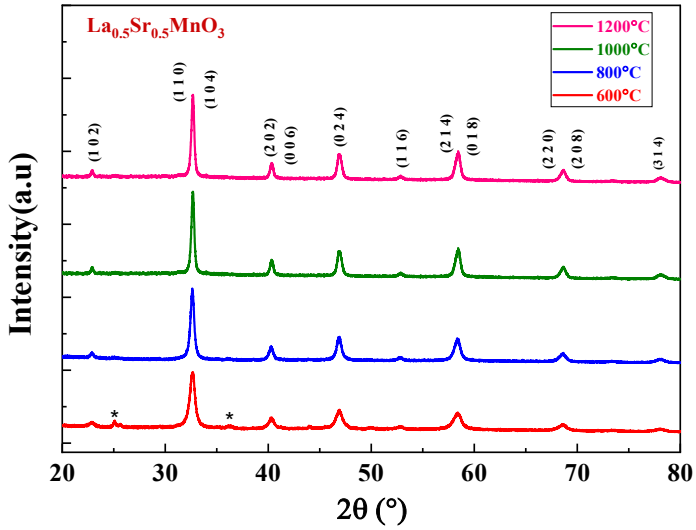

Figure 1: XRD pattern of $La_{0.5}Sr_{0.5}MnO_3$ nanocrystallites annealed 600°C, 800°C, 1000°C and 1200°C.

The variation of crystallite size of $La_{0.5}Sr_{0.5}MnO_3$ nanocrystalline were presented from the Table 1, known that the size of the crystallites increases from 15 to 30nm when the annealed from 600°C to 1200°C. This indicates that the $La_{0.5}Sr_{0.5}MnO_3$ perovskite structure has a high level of crystallinity, with all its peaks present and without any impurities or phases observed above 600°C.

Table 1: Structural and Optical parameters of the $La_{0.5}Sr_{0.5}MnO_3$ nanoparticles annealed at 600°C, 800°C,1000°C and 1200°C.

Annealing Temperature	**600°C**	**800°C**	**1000°C**	**1200°C**
Crystallite Size D (nm)	15	18	22	30
Dislocation density (δ_D) (nm^{-2})×10^{-3}	4.44	3.08	2.06	1.04
Micro strain (ε)×10^{-3}	8.74	6.10	5.06	4.63
Absorption peak (nm)	392	393	398	420
Band gap (eV)	3.02	2.64	2.53	2.48
Refractive Index (By Moss Relation)	2.36	2.44	2.47	2.48
Refractive Index (By Herve and Vandamme)	2.39	2.46	2.49	2.50
Static dielectric constant (ε_o)	9.21	10.38	10.72	10.88
High frequency dielectric constant (ε_α)	5.57	5.95	6.10	6.15

The crystal defects can be measured by the dislocation density(δ_D) ,which was measured from Williamson and Smallman's relation given by equation (2) and the micro-strain (ε) were evaluated by below relations (3) [26].

$$\delta_D = \frac{1}{D^2} \quad \ldots\ldots\ldots\ldots\ldots\ldots\ldots (2)$$

$$\varepsilon = \frac{\beta}{4\tan\theta} \quad \ldots\ldots\ldots\ldots\ldots\ldots\ldots (3)$$

The values of δ_D and ε are shown in Table 1. From this, dislocation density and microstrian reduces due to increase in the crystallite size.

UV-vis spectroscopy Analysis: Figures 2(a) and 2(b) display the UV-visible absorbance and transmittance spectra of the post annealed $La_{0.5}Sr_{0.5}MnO_3$ nanocrystallites. The optical absorption spectra exhibit a non-linear form, suggesting that the absorption of visible light is not due to a transition from impurity levels, but rather arises from a transition within the bandgap.

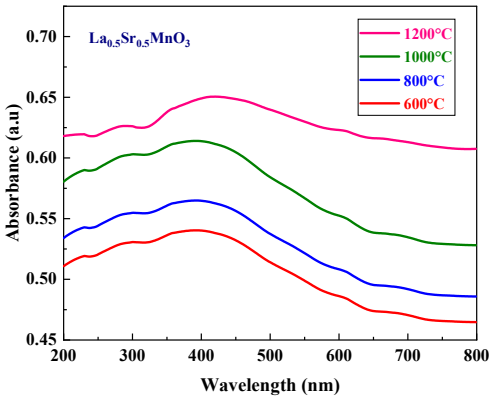

Figure: 2(a)

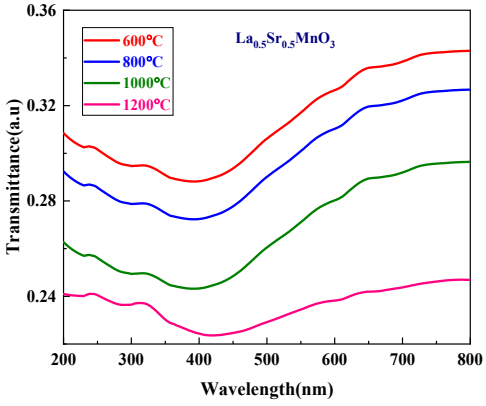

Figure: 2(b)

Figure 2(a-b): Uv-vis Absorbance and Transmittance spectra of $La_{0.5}Sr_{0.5}MnO_3$ nanocrystallites annealed at 600°C, 800°C, 1000°C, and 1200 °C.

Analysis of Figure 2(a) reveals that all samples have a UV cut-off point at 300 nm, and there is significant absorption within the 320-420 nm range. The spectrum clearly shows that

maximum absorbance peaks were at 392, 393, 398, 420nm for the nanocrystallites annealed 600℃, 800℃, 1000℃, and 1200℃ with absorbance of 54%, 56%, 61%, 65%. It clearly shows that the absorbance percentage and maximum absorbance wavelength values increases with annealing temperature. Not much variation is observed for the sample at 1200℃ in the range 500 to 800nm.

$La_{0.5}Sr_{0.5}MnO_3$ nanocrystallites' absorbance coefficient was determined using Beer- Lambert's Law. [27,28].

$$I = I_0 e^{\alpha t} \ldots\ldots\ldots\ldots\ldots\ldots (4)$$

$$A = log\left(\frac{I_0}{I}\right) \ldots\ldots\ldots\ldots\ldots\ldots (5)$$

$$\alpha = \frac{2.303\, A}{t} \ldots\ldots\ldots\ldots\ldots\ldots\ldots (6)$$

Where I_0 and I represent the intensity of incident and transmitted radiation , 'α' and 'A' represents coefficient of absorption and absorbance respectively. 't' represents length of the sample holder (=1cm).

$La_{0.5}Sr_{0.5}MnO_3$ nanocrystallites' transmittance (T_s) is estimated using the relation.

$$T_s = 10^{-A} \times 100 \ldots\ldots\ldots\ldots\ldots (7)$$

The transmittance verses wavelength curve displayed typical generated interference fringes, a nonlinear reduction in shorter wavelength region, and high transparency response throughout the whole investigated spectral range. A red-shift of the transmittance-curve edge can be observed and transmittance value decreases from 0.28 to 0.22 as increases as rise of annealing temperature from 600℃ to 1200℃.

The reflectance of all nanocrystallites was evaluated by the formula [29].

$$R = \frac{(n-1)^2}{(n+1)^2} \ldots\ldots\ldots\ldots\ldots\ldots (8)$$

Where 'n' is the refractive index measured by the relation, $n = \frac{1}{T_s} + \sqrt{\frac{1}{T_s - 1}}$

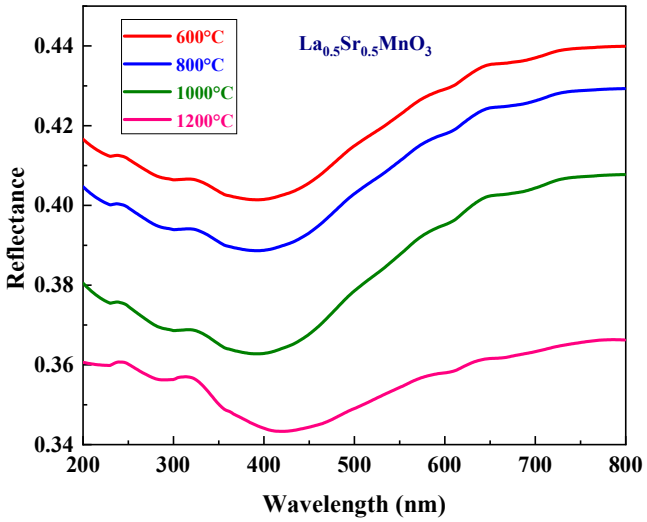

Figure 3: Uv-vis Reflectance spectra of $La_{0.5}Sr_{0.5}MnO_3$ nanocrystallites annealed at 600°C, 800°C, 1000°C, and 1200°C.

The UV-visible reflectance spectrum of all nanocrystallites is shown in Figure 3, demonstrates that the nanocrystallites have an excellent optical reflectance of 35– 45% from 600 to 800nm and minimum reflectance were observed in the wavelength region 390 – 430nm.In the reflectance spectrum of samples the minimum reflectance value decreases from 0.40 at 393nm to 0.34 at 413nm on increasing of annealing temperature.

Band gap energy measurement:

In general, the Tauc's relation [28] connects photon energy (hυ) with the absorption coefficient (α). The type of optical transition is determined by the below expression,

$$\alpha h\nu = A\left(h\nu - E_g\right)^m \dots\dots\dots\dots\dots\dots (8)$$

where A and E_g are the constant and the optical band gap respectively. 'm' is the factor, decides the nature of optical transition. The values of 'm' is 1/2 for direct allowed, 3/2 for forbidden transitions, 2 for indirect allowed and 3 for forbidden transition. The determination of the transition type involves finding the value of m. To accomplish this, Equation (8) can be rearranged as:

$$ln(\alpha h\nu) = ln(A) + m\, ln\left(h\nu - E_g\right) \dots\dots\dots\dots\dots (9)$$

By plotting the curve of $\ln(\alpha h\nu)$ versus $\ln\left(h\nu - E_g\right)$ the value of m can be determined. In this study, the obtained value of m was approximately 1/2, indicating an electronic transition from the valence band to the conduction band, accompanied by strong electronic absorption. Consequently, a more precise value was derived from the straight-line portion of the graph $(\alpha h\nu)^2$versus $(h\nu)$, indicating a direct transition within the broad band gap region. Extrapolating this straight line allowed for the determination of the intercept on the (hν)-axis, providing the value of the direct optical gap (E_g).

Table 1 presents the direct band gap values of $La_{0.5}Sr_{0.5}MnO_3$ nanocrystallites after undergoing annealing. The data indicates that the optical gap decreases from 3.02eV to 2.48eV as the annealing temperature increases. The decrease in the band gap, known as a "red shift," can be ascribed to an increase in particle size, which is consistent with the XRD results. The observed band gap values suggest that "these compounds have the potential to be used in new high-frequency optoelectronic devices. Materials with a band gap energy greater than 2 eV are particularly interesting for applications in the UV region of the electromagnetic spectrum" [30,31]. Furthermore, based on the band gap energy values and the semiconductor nature exhibited by the prepared samples, they are considered promising options for photocatalytic activities.

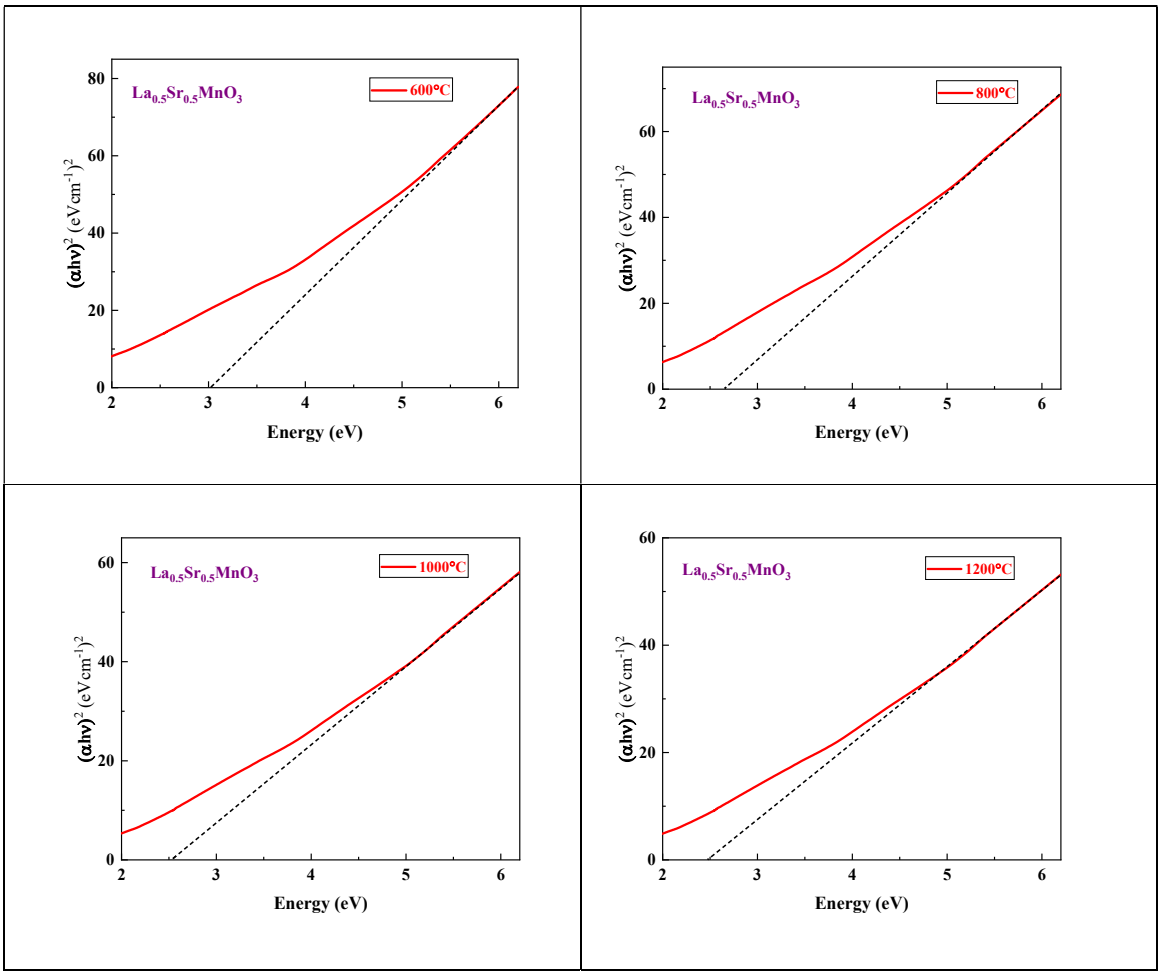

Figure 4: UV-Vis absorbance -Tauc plot: Variation of $(\alpha h\nu)^2$ versus photon energy "hv" of $La_{0.5}Sr_{0.5}MnO_3$ nanocrystallites annealed at 600°C, 800°C, 1000°C, and 1200°C.

The measurement of refractive index from energy gap:

The optical and electronic properties of semiconductors can be characterized by two important physical parameters: the refractive index and the optical gap. The refractive index (n) of the samples obtained in this study is determined using the Moss relation [32,33], which can be expressed as follows:

$$n^4 E_g = 95eV \ldots\ldots\ldots\ldots\ldots\ldots (10)$$

where E_g is the energy band gap. This model is derived from Bohr's atomic model of hydrogen and applies to solids. The underlying assumption is that all energy levels within a solid are reduced in size by a factor of $\frac{1}{\epsilon_\infty^2}$, where ϵ_∞ represents the optical dielectric constant that satisfies the relation $\epsilon_\infty = n^2$.

Herve and Vandamme stated another relation to find the refractive index as [34]

$$n = \sqrt{1 + \left(\frac{A}{E_g + B}\right)^2} \ldots\ldots\ldots\ldots\ldots\ldots\ldots (11)$$

where A=13.6eV and B=3.4eV are the hydrogen ionization energy with values. Table 1 presents the refractive index (n) values for all the samples, illustrating the variations observed under two different models. The data clearly demonstrates that the refractive index increases as the annealing temperatures are raised. However, it is important to note that the rate of this change is dependent on the specific model employed. The static dielectric constant (ε_o) and high frequency dielectric constant (ε_α) of all samples are determined using the following relation (8) and (9) [33].

$$\varepsilon_o = 18.52 - 3.08E_g \dots\dots\dots\dots\dots\dots (8)$$

$$\varepsilon_\alpha = n^2 \dots\dots\dots\dots\dots\dots\dots (9)$$

The values of static dielectric constant (ε_o) and high frequency dielectric constant (ε_α) of all samples are shown in Table1, reveals that static dielectric constant increases and high frequency dielectric constant decreases with the annealing temperature.

Conclusion:

The combustion method was successfully used to synthesize $La_{0.5}Sr_{0.5}MnO_3$ nanocrystals The XRD confirmed the structure of Rhombohedral, $3\bar{R}C$ space group. As the annealing temperature increased, the crystallite sizes of the $La_{0.5}Sr_{0.5}MnO_3$ nanocrystals increased from 15 to 30nm, while the micro strain decreased from 8.74×10^{-3} to 4.63×10^{-3}, and the dislocation density were reduced from 4.44×10^{-3} nm^{-2} to 1.04×10^{-3} nm^{-2} .The absorbance spectrum clearly shows that maximum absorbance peaks were at 392, 393, 398, 420nm with absorbance of 54%, 56%, 61%, 65% for samples annealed at 600℃, 800℃, 1000℃ and 1200℃. The nanocrystallites hold a decent optical reflectance of 35– 45% from 600 to 800nm and minimum reflectance were observed in the wavelength region 390 – 430nm. The optical band gap values were changed from 3.02eV to 2.48eV as the crystallite size increased, suggesting that the $La_{0.5}Sr_{0.5}MnO_3$ nanoparticles were semiconductor in nature. The refractive index value of all samples increases from 2.36 to 2.48 (measured by Moss relation) and from 2.39 to 2.50 (measured by Herve and Vandamme) with increase annealing temperatures. For all the static dielectric constant increases and high frequency dielectric constant decreases with the annealing temperature.

References:

[1] J.M.D. Coey, M. Viret, S. von Molnar, Mixed-valence manganites, Adv. Phys. 48 (1999) 167–293.

[2] C.A. Hancock, J.M. Porras-Vazquez, P.J. Keenan, P.R. Slater, Oxyanions in perovskites: from superconductors to solid oxide fuel cells, Dalton Trans. 44 (2015) 10559–10569.

[3] S. Jin, T.H. Tiefel, M. McCormack, R.A. Fastnacht, R. Ramesh, L.H. Chen, Thousandfold change in resistivity in magnetoresistive La-Ca-Mn-O films, Science 264 (1994) 413–415.

[4] P. Ciambelli, S. Cimino, S.D. Rossi, M. Faticanti, L. Lisi, G. Minelli, I. Pettiti,P. Porta, G. Russ, M. Turco, AMnO3 (A¼La, Nd, Sm) and Sm1-xSrxMnO3 perovskites combustion catalysts: structural, redox and catalytic properties, Appl. Catal. B Environ. 24 (2001) 243–253.

[5] K.P. Shinde, S.S. Pawara, N.G. Deshpande, J.M. Kim, Y.P. Lee, S.H. Pawar, Magnetocaloric effect in LSMO synthesized by combustion route, Mater. Chem. Phys. 129 (2011) 180–182.
[6] B. Raveau, A. Maignan, C. Martin, Insulator–metal transition induced by Cr and Co doping in Pr0.5Ca0.5MnO3, J. Solid State Chem. 130 (1997) 162–166.
[7] D. Liu, N. Wang, G. Wang, Z. Shao, X. Zhu, C. Zhang, H. Cheng, Programmable metallization cells based on amorphous La0.79Sr0.21MnO3 thin films for memory applications, J. Alloys Compd. 580 (2013) 354–357.
[8] S. Liu, B. Guillet, A. Aryan, C. Adamo, C. Fur, J.M. Routoure, F. Lemarie, D. G. Schlom, L. Mechin, La0.7Sr0.3MnO3 suspended microbridges for uncooled bolometers made using reactive ion etching of the silicon substrates, Microelectron. Eng. 111 (2013) 101–104.
[9] F. Dong, D. Chen, R. Ran, H. Park, C. Kwak, Z. Shao, A comparative study of Sm0.5Sr0.5MO3-δ (M¼Co and Mn) as oxygen reduction electrodes for solid oxide fuel cells, Int. J. Hydrogen Energy 37 (2012) 4377–43877.
[10] Y. Tokura, Critical features of colossal magnetoresistive manganites, Rep. Prog. Phys. 69 (2006) 797–851.
[11] Investigation on the structural, magnetic and magnetocaloric properties of nanocrystalline Pr-deficient $Pr_{1-x}Sr_xMnO_{3-\delta}$ manganites, J. Magn. Magn Mater. 448 (2018) 322–331.
[12] L. Chen, J. Fan, W. Tong, D. Hu, Y. Ji, J. Liu, L. Zhang, L. Pi, Y. Zhang, H. Yang, Evolution of the intrinsic electronic phase separation in La0.6Er0.1Sr0.3MnO3 perovskite, Sci. Rep. 6 (2016) 14–22.
[13] A.V. Golenishchev-Kutuzov, V.A. Golenishchev-Kutuzov, R.I. Kalimullin, A. V. Semennikov, Ordered states of Jahn–Teller distorted MnO6 octahedra in weakly doped lanthanum–strontium manganites, Phys. Solid State 57 (2015) 1633–1638.
[14] A.K. Sahu, A. Ghosh, A.K. Suri, Characterization of porous lanthanum strontium manganite (LSM) and development of yttria stabilized zirconia (YSZ) coating, Ceram. Int. 35 (2009) 2493–2497.
[15] A.O. Turky, M.M. Rashaa, A.M. Hassan, E.M. Elnaggar, M. Bechelany, Tailoring optical, magnetic and electric behavior of lanthanum strontium manganite La1- xSrxMnO3 (LSM) nanopowders prepared via co-precipitation method with different Sr2þ ion contents, RSC Adv. 6 (2016) 17980–17986.
[16] J. Hemberger, A. Krimmel, T. Kurz, H.A.K. Von Nidda, V.Y. Ivanov, A.A. Mukhin, A.M. Balbashov, A. Loidl, Structural, magnetic, and electrical properties of single - crystalline $La_{1-x}Sr_xMnO_3$ ($0.4<x<0.85$), Phys. Rev. B 66 (2002) 944101–944108.
[17] A. Urushibara, Y. Moritomo, T. Arima, A. Asamitsu, G. Kido, and Y. Tokura, "Insulator-metal transition and giant magnetoresistance in $La_{1-x}Sr_xMnO_3$", Phys. Rev. B 51, 14103 (1995).
[18] Patil, S. I. and Bhagat, S. M. and Shu, Q. Q. and Lofland, S. E.et al., "Indications of phase separation in polycrystalline La1−xSrxMnO3 for x≈0.5". Phys. Rev. B **62**, 9548 (2000).
[19] Jirák, Z, Hejtmanek, Jiri, Maryško, M, Sonntag, R. (2000). "Ferromagnetic–antiferromagnetic transition in tetragonal $La_{0.50}Sr_{0.5}0MnO_3$". Journal of Magnetism and Magnetic Materials. 217. 113–119. 10.1016/S0304-8853(00)00326-7.

[20] Chmaissem, O. Dabrowski, B. Kolesnik, S. Mais, J. Jorgensen, J. D. Short, S. "Structural and magnetic phase diagrams of La1−xSrxMnO3 and Pr1−ySryMnO3". Phys. Rev. B **67**, 094431 (2003).
[21] S. M. Zhou, L. Shi, H. P. Yang, Y. Wang, L. F. He, and J. Y. Zhao "Size-dependent exchange bias in half-doped manganite nanoparticles", Appl. Phys. Lett. 93, 182509 (2008).
[22] T. Zhang and M. Dressel, "Grain-size effects on the charge ordering and exchange bias in Pr0.5Ca0.5MnO3: The role of spin configuration", Phys. Rev. B 80, 014435 (2009).
[23] Bokov, D.; Jalil, A. T.; Chupradit, S.; Suksatan, W.; Ansari, M. J.; Shewael, I. H.; Gabdrakhman.; Valiv, H.; Kainfar, E. 2021, "Nanomaterial by Sol-Gel Method: synthesis and Application". Adv. Mat. Sci. Eng. 2021, 21.
[24] Kamegashira, N.; Miyazaki, Y.; Yamamoto, H.; Yamamoto, H. Oxygen pressures over LaMnO3+. *Materials Chemis try and Physics II*. **1984**, 181-194.
[25] Lipham, N. D.; Tsoi, G.M.; Wenger, L. E. Synthesis and Characterization of Sr-Doped Lanthanum Manganite Nanoparticles. *IEEE Transactions on Magnetics*. **2007**,*43*,3088-3090.
[26] Pawar, D.K.; Pawar, S.M.; Patil, P.S.; Kolekar, S.S. Synthesis of Nano-crystalline Nickel-Zinc Ferrite (Ni0.8n0.2Fe2O4) Thin Films by Chemical Bath De- Position Method *J Alloy Compd*. **2011**, *509*,3587-3591.
[27] Pathan, H.M., Desai, J.D. and Lokhande, C.D. (2002) Modified Chemical Deposition and Physico- Chemical Properties of Copper Sulphide (Cu2S) Thin Films. Applied Surface Science, 202,47-56.
[28] Srivastava, M., Ojha, A.K., Chaubey, S. and Materny, A. (2009) Synthesis and Optical Characterization of Nanocrystalline NiFe2O4 Structures. Journal of Alloys and Compounds, 481,515-519.
[29] A. Ashour, N. El-Kadry, S.A. Mahmoud, the electrical and optical properties of CdS films thermally deposited by a modified source, Thin solid films (1995), 269,117-120.
[30] M. P. de Jong, V. A. Dediu, C. Taliani and W. R. Salaneck, Journal of Applied Physics, 2003, 94, 7292-7296.
[31] K. Takenaka, Y. Sawaki, R. Shiozaki and S. Sugai, Physical Review B, 2000, 62, 13864-13867.
[32] Moss T.S. Photoconductivity in the Elements. *Proc. Phys. Soc. Sect. A.* 1951;64:590–591. doi: 10.1088/0370-1298/64/6/113.
[33] Moss T.S. Relations between the Refractive Index and Energy Gap of Semiconductors. *Phys. Status Solidi (b)* 1985;131:415–427. doi: 10.1002/pssb.2221310202.
[34] P. Herve and L. K. J. Vandamme, General Relation between Refractive-Index and Energy-Gap in Semiconductors, Infrared Phys. Technol., 1994, 35, 609–615.